
A SIMPLE TEST-TIME METHOD FOR OUT-OF-DISTRIBUTION DETECTION

Ke Fan

School of Data Science
Fudan University
Shanghai
kfan21@m.fudan.edu.cn

Yikai Wang

School of Data Science
Fudan University
Shanghai
yikaiwang19@fudan.edu.cn

Qian Yu

Beihang University
Beijing
qianyu@buaa.edu.cn

Da Li

Samsung AI Center
Cambridge
dali.academic@gmail.com

Yanwei Fu

School of Data Science
Fudan University
Shanghai
yanweifu@fudan.edu.cn

ABSTRACT

Neural networks are known to produce over-confident predictions on input images, even when these images are out-of-distribution (OOD) samples. This limits the applications of neural network models in real-world scenarios, where OOD samples exist. Many existing approaches identify the OOD instances via exploiting various cues, such as finding irregular patterns in the feature space, logits space, gradient space or the raw space of images. In contrast, this paper proposes a simple Test-time Linear Training (ETLT) method for OOD detection. Empirically, we find that the probabilities of input images being out-of-distribution are surprisingly linearly correlated to the features extracted by neural networks. To be specific, many state-of-the-art OOD algorithms, although designed to measure reliability in different ways, actually lead to OOD scores mostly linearly related to their image features. Thus, by simply learning a linear regression model trained from the paired image features and inferred OOD scores at test-time, we can make a more precise OOD prediction for the test instances. We further propose an online variant of the proposed method, which achieves promising performance and is more practical in real-world applications. Remarkably, we improve FPR95 from 51.37% to 12.30% on CIFAR-10 datasets with maximum softmax probability as the base OOD detector. Extensive experiments on several benchmark datasets show the efficacy of ETLT for OOD detection task.

1 Introduction

Deep neural networks are known to achieve outstanding performance on image recognition tasks [1, 2, 3, 4]. However, the model prediction is only trustable when the input data follows the distribution of the training dataset. When the input data is far away from the training data, the neural networks are inclined to make arbitrarily over-confident predictions [5, 6], hindering the reliability of the deep model in realistic applications.

To tackle this problem, many techniques [7, 8, 9, 10, 11, 12, 13, 14] have been proposed to facilitate the trained models to recognize those irregular input data and reject to provide predictions. Specifically, the training data distribution is modelled as the in-distribution, while those irregular data are assumed from the out-of-distribution (OOD). It is the primary goal of differentiating the two types of data, i.e., detecting the out-of-distribution data. So far, in the literature, OOD samples are typically detected by distinguishing irregular patterns existed in the feature space [10, 11, 12], logit space [7, 14], gradient space [13], etc. For example, maximum softmax probability [7] and Helmholtz free energy [9] methods are based on the predicted logits and Mahalanobis distance OOD detector [10] is based on the extracted features.

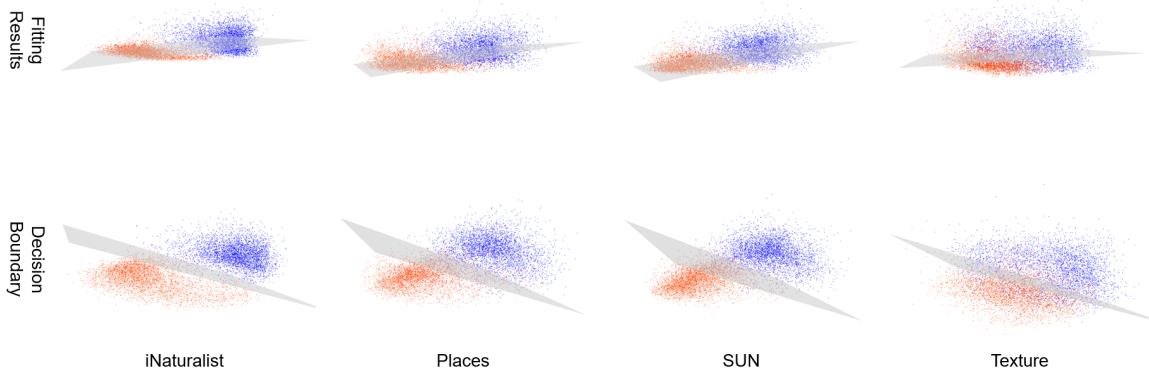


Figure 1: Illustration of the linear relationship between features and OOD scores (EBM energy) of ImageNet (in-distribution) and four OOD datasets. *Blue/orange* points denote *in/out-of-distribution* features. Features were extracted using pre-trained ResNet-101 and reduced to dimension 2 by PCA for visualization. Critically, the image was visualized in 3D space (not using 2D points). We first draw a 3D scatter plot with the reduced feature (x, y) and OOD score z as coordinates, then fit a linear regression and a SVM (assume access to the ground truth labels) via the grey hyper-plane. The upper row fits a linear regression model and displays the fitted OOD score via the grey hyper-plane, indicating a roughly linear relationship between OOD scores and features. The lower row presents the fitted decision boundary between in- and out-of-distribution data, suggesting a linear separable feature pattern.

For the current OOD detection benchmarks, the test dataset is typically a mixture of test data from the in-distribution and some data from a distinct dataset [10, 7, 14, 8, 15]. In this paper, we show that under such a setup the in-distribution and out-of-distribution data is actually nearly linear-separable as shown in Fig. 1. It can be seen that the in-distribution data of ImageNet (blue dots) are roughly linearly separable from the out-of-distribution data (orange dots).

This linear separability is consistently observed across different OOD datasets.

More interestingly, Figure 1 conveys that there is an approximated linear relation, which may be learned directly, between the features extracted by the pretrained neural network and the predicted OOD scores generated by different OOD algorithms. We find then a simple linear regression learned to fit the extracted features and inferred OOD scores can yield more accurate OOD scores than the used base OOD detection algorithms.

Based on this observation, we propose an Embarrassingly simple Test-Time Linear Training (ETLT) model to tackle OOD detection problem at test time. We model the linear relation between features and OOD scores and provide the rectified OOD score directly based on the input feature. Specifically, we present two variants of ETLT to handle different scenarios: When the feature-score pairs provide strong enough linear relation, a simple Direct Linear Regression (DLR) algorithm is used to learn and produce revised OOD scores. When the linear relation is less recognisable due to some detection errors introduced by the base OOD detection algorithms, we introduce a Robust Linear Regression (RLR) model to discover the true linear relation from those noisy pairs. Moreover, DLR can be easily implemented as an online version, which is more practical to real-world applications. We conduct extensive experiments and show the effectiveness of our ETLT across different datasets and over different base OOD detection algorithms.

Our contributions are as follows:

- We show that there exists a roughly linear separation between the in- and out-of-distribution data according to the existing OOD detection evaluation setup. And we observe a linear relation between the extracted features and the OOD scores inferred by those popular OOD detection methods.
- We then propose an embarrassingly simple test-time linear training model, including two variants, a simple Direct Linear Regression (DLR) and a Robust Linear Regression (RLR), to discover and use this linear relation to provide revised OOD scores directly based on the input features. We further derive an online version of DLR, which is more practical and produce as good results as DLR.
- Our ETLT algorithm enjoys the state-of-the-art performance on various benchmark datasets and improves over four popular base OOD detection methods.

2 Related Work

Out-Of-Distribution Detection Analogous to detecting misclassified examples, a baseline of OOD detection was proposed in [7] by using the maximum softmax probability (MSP) produced by the trained neural networks. Inspired by the idea of adversarial examples [16], an input preprocessing method named ODIN [14] was proposed to improve MSP. Furthermore, Mahalanobis distance based class-conditional confidence score for OOD detection was proposed in [10] under the modeling of Gaussian discriminant analysis. Though achieving great improvements over MSP, the followup ODIN and Mahalanobis detectors need hyperparameter optimization on a validation set or in-distribution set, which is prohibitive in many cases. To overcome such a drawback, Energy-based score serving as a parameter-free OOD detector was proposed in [9]. Recently, GradNorm was proposed in [13] by exploring the gradient information of minimizing the KL discrepancy between the predicted posterior and the uniform distribution. All the methods above can be applied on top of any pre-trained classification network trained with a cross entropy loss.

Another class of OOD detectors attack on OOD problem by training specifically designed networks [17, 8]. A confidence estimation branch, in addition to the task branch, was proposed in [17]. Similarly, Generalized ODIN [8] learned separate branches for modeling the joint class-domain probability and domain probability respectively as a decomposition of the confidence scoring, while in this way the temperature scaling could be automatically learned.

Additionally, Outlier Exposure(OE) [18] leveraged an auxiliary OOD dataset to train an OOD detector directly. Out-of-Distribution Mining (ODM) [19] proposed to use metric learning to get rid of the (trouble-maker) softmax layer. ATOM [20] applied adversarial training to shrink the decision boundary between in-distribution dataset and auxiliary OOD dataset to achieve better results. Recently, self-supervised learning had been combined with outlier exposure [21]. Furthermore, directly controlling the difference between in- and out-of-distribution samples was proved to further separate them [22].

Test-Time Adaptation (TTA). TTA [23, 24, 25] was introduced to alleviate the distributional shift problem between the training and testing data, as deep models are known to be biased to the training data distribution and could fail predicting correctly on the test data from an unseen distribution. TTA adapts the trained models to the novel data during testing by updating its parameters with the mini-batch [23, 24] or full [25] unlabeled test data. TTA approaches chose to update batch-norm parameters/statistics to fit the testing data [24, 26], or minimize the prediction inconsistency [27] between different data augmentation of a single data point. Our ETLT conceptually follows the TTA setup in the way that we have access to the mini-batch or full test data. However, we focus on using the inferred OOD signal at test and the linear relation between features and OOD scores to improve OOD detection, rather than model adaptation in the standard TTA. The difference between TTA and Transductive Learning(TL) is that TL is learned on train and test data jointly, while the model for TTA is updated by unlabeled test data at test time as in [24]

Outlier Detection. Irregular data are also considered in some other research fields. Outlier detection [28] assumes that the data are polluted by outliers. Generally, OOD detectors process a single sample at a time while outlier detectors assume the accessibility to all the testing samples. When evaluating OOD detection in the TTA setup, the two settings get similar. Therefore, we also compare our algorithms with some outlier detection methods.

3 Methodology

Problem setup. In the traditional supervised image classification tasks, one typically learns a mapping $f : \mathcal{X} \rightarrow \mathcal{Y}$ from image space $\mathcal{X} \subseteq \mathbb{R}^m$ to label space $\mathcal{Y} = \{1, 2, \dots, C\}$ with a given training set $D = \{(\mathbf{x}_i, y_i)\}_{i=1}^n$. Then at inference, the predicted label can be achieved according to the maximum score $\hat{y} = \operatorname{argmax} f(\mathbf{x})$.

In practice, there exists ‘unexpected’ data that is far away from the training set, and for the sake of model reliability those data samples should be rejected without obtaining any predictions. Formally, we assume that the training data is drawn from the distribution P_{in} , which we call in-distribution, and those unexpected data are drawn from a distinct out-distribution P_{out} . Precisely, we assume a mixture distribution P_{mix} defined on $\mathcal{X} \times \mathcal{Z}$, where $\mathcal{Z} = \{0, 1\}$, $P_{mix}(X|Z=0) = P_{in}(X)$ and $P_{mix}(X|Z=1) = P_{out}(X)$. Out-of-distribution detection aims at distinguishing which distribution $\mathbf{x} \sim P_{mix}$ is drawn from.

In general, the OOD detection problem can be viewed as a binary classification problem with only in-distribution data available during training. However, such a binary decision is hard to achieve in practice. Instead, the continuous OOD scores are usually exploited for OOD detection in the way that the model could reject unreliable instances if their scores are below a proper threshold. Specifically, for each \mathbf{x} we provide an OOD score estimator $S(\mathbf{x})$ and design a binary classifier with manually-defined threshold γ :

$$g(\mathbf{x}) = \begin{cases} \text{in}, & \text{if } S(\mathbf{x}) \geq \gamma, \\ \text{out}, & \text{if } S(\mathbf{x}) < \gamma. \end{cases} \quad (1)$$

Here we review several recent **OOD score** based methods:

MSP. The maximum softmax probability [7] is defined as OOD score given by a trained network

$$S_{\text{MSP}}(\mathbf{x}) := \frac{\exp(f_{\hat{y}}(\mathbf{x})/T)}{\sum_{j=1}^C \exp(f_j(\mathbf{x})/T)}, \quad (2)$$

where T is the temperature coefficient introduced in [14] to make the softmax prediction sharp. Vanilla MSP [7] did not include temperature scaling, which was proposed in ODIN [14]. For the ease of our overall formulation we add it here.

Energy. Energy-based model (EBM) [29] aims to find a suitable energy function $E(x, y)$ defined on $\mathcal{X} \times \mathcal{Y}$, and model the posterior probability by the Gibbs distribution

$$p(y | \mathbf{x}) = \frac{\exp(-E(\mathbf{x}, y)/T)}{\exp(-E(\mathbf{x})/T)}. \quad (3)$$

The Helmholtz free energy $E(\mathbf{x})$ of a given data point \mathbf{x} can be expressed as the negative of the log partition function

$$E(\mathbf{x}) = -T \cdot \log \int_{y'} \exp(-E(\mathbf{x}, y')/T). \quad (4)$$

The Helmholtz free energy for $\mathbf{x} \sim P_{in}$ is push down during the training process, and therefore can serve as an alternative metric for OOD detection [9]. More details of EBM can be found in [29]. Direct connecting Helmholtz free energy with softmax probability, we get another baseline OOD detector:

$$S_{\text{energy}}(\mathbf{x}) := -E(\mathbf{x}) = T \cdot \log \sum_i^C \exp(f_i(\mathbf{x})/T). \quad (5)$$

KL. An in-distribution sample should tend to have a prediction with the minimum entropy, while an OOD data is not properly defined in the training label space and should be predicted with large predictive entropy. Therefore, the Kullback-Leibler (KL) divergence between the softmax output and a uniform distribution is proposed in [15] to improve the OOD scoring

$$\begin{aligned} S_{\text{KL}}(\mathbf{x}) &:= D_{\text{KL}}(\mathbf{u} \parallel \text{SoftMax}(f(\mathbf{x}))) \\ &= -\frac{1}{C} \sum_{i=1}^C \log \frac{\exp(f_i(\mathbf{x})/T)}{\sum_{j=1}^C \exp(f_j(\mathbf{x})/T)} - H(\mathbf{u}) \end{aligned} \quad (6)$$

where $\mathbf{u} = [1/C, 1/C, \dots, 1/C] \in \mathbb{R}^C$ is a uniform probability and $H(\mathbf{u}) = \log C$. Since we focus on the OOD score, thus the constant term could be dropped.

ODIN. ODIN [14] got the inspiration from adversarial attack [16] and find that including the adversarial perturbed inputs into training improves the final OOD scoring. Given an input image \mathbf{x} and the predicted softmax probability, ODIN first generates the perturbed image by

$$\tilde{\mathbf{x}} = \mathbf{x} - \varepsilon \text{sign}(-\nabla_{\mathbf{x}} \log S_{\text{MSP}}(\mathbf{x})), \quad (7)$$

then the MSP of the perturbed image will be maximized during training. At test time, the perturbed image $\tilde{\mathbf{x}}$ is used to produce the final OOD score as

$$S_{\text{ODIN}}(\mathbf{x}) = S_{\text{MSP}}(\tilde{\mathbf{x}}). \quad (8)$$

In the following, we will demonstrate a linear relation between the extracted features and inferred scores at test time and learn a linear regression to improve the above four base OOD detection methods.

3.1 The Surprisingly Linear Relation

We think that the above four OOD scores are likely to be sub-optimal, because they only deal with a single sample at a time and ignore the interaction between samples.

In this paper, we show that with a mini-batch (full) test data in hand, we can improve the baseline OOD methods significantly. Although there is a certain number of wrongly inferred OOD scores of the test data, i.e. the OOD samples over-confidently predicted by the trained model, training a linear regression is still able to rectify those overconfident (noisy) scores.

We empirically observe that a simple linear relationship exists between the feature extracted from the neural network and the inferred OOD scores by those base OOD detection algorithms, as shown in Fig. 1. Furthermore, the in- and

out-of-distribution features are linear-separable. We also give a 2D visualization in Fig. 3. Although those OOD scores are from different (nonlinear) scoring algorithms, the input features and OOD scores are well fitted with a linear regression.

We thought this roughly linear relation is quite intuitive, as it is just a direct linear approximation to Generalized Linear Model (GLM). Particularly, the typical OOD methods such as MSP has a backbone and softmax-based classification header and an OOD scorer. As softmax function is a typical GLM, the relationship of softmax-based classification head and OOD score can be taken as roughly GLM. During training stage, the model should be trained to match the classifier head and feature backbone. Therefore, the linear relation between feature and OOD score is established as a consequence of an approximation of the GLM. Based on this empirical observation, we propose a simple method, which enjoys nearly no extra cost, to improve the current OOD detection methods.

3.2 Simple Test-Time Linear Training

Let us denote the (un-normalized) OOD score of an input image as $s := S(\mathbf{x})$. We assume a linear relation between the OOD score s and the input feature \mathbf{z} extracted by the trained model:

$$s = \mathbf{z}^\top \beta + \varepsilon. \quad (9)$$

For a particular OOD algorithm ω , it will produce a (noisy) estimation \hat{s}_i of s_i based on the input image \mathbf{x}_i , resulting $\hat{s}_i := S_\omega(\mathbf{x}_i)$. We aim to discover the *true* β from the feature-score pair $(\mathbf{z}_i, \hat{s}_i)$, hence we can get a more precise estimation of s_i .

We consider two slightly different test-time linear training methods. Particularly, when a set of test instances are embedded with a small amount of noisy scores, a simple linear regression model could be well fitted.

On the other hand, if the amount of noisy samples is too large to train a linear model, we will introduce a robust variant which generates the noise scores such that a clean set could be selected. The details of two models are introduced as follows.

Direct Linear Regression (DLR). When linear relation is recognisable, a simple linear regression model is sufficient to estimate the true β such that:

$$\hat{\beta} = \operatorname{argmin}_{\beta} \sum_{i=1}^n (\hat{s}_i - \mathbf{z}_i^\top \beta)^2, \quad (10)$$

which yields the closed-form solution

$$\hat{\beta} = (\mathbf{Z}^\top \mathbf{Z})^\dagger \mathbf{Z}^\top \hat{\mathbf{S}}, \quad (11)$$

where \mathbf{Z} and $\hat{\mathbf{S}}$ are the stack of \mathbf{z}_i and \hat{s}_i by rows, respectively. With this estimator, we could directly provide our OOD estimator for instance i as:

$$\hat{s}_{\text{ours}} = \mathbf{z}_i^\top \hat{\beta}. \quad (12)$$

Robust Linear Regression (RLR). When the originally inferred OOD scores are too noisy caused by the OOD scoring method ω , we can design another outlier detection model to remove those noisy data from estimating β .

Specifically, we introduce an explicit data-dependent variable γ_i to represent the prediction error of the linear regression model, such that

$$\hat{s}_i = \mathbf{z}_i^\top \beta + \gamma_i + \varepsilon. \quad (13)$$

When $|\gamma_i|$ is small, the linear relation is preserved, indicating that instance i is helpful to guide the estimation of β . On the contrary, when $|\gamma_i|$ is large, the corresponding instance should be ignored as the estimated \hat{s}_i is likely to be wrong.

Note that in this robust variant, we aim to detect the noisy instances instead of predicting β , hence we only care about the solution of γ_i . Based on this intuition, we design the following optimization problem:

$$\min_{\beta, \gamma} \sum_{i=1}^n \left[\frac{1}{2} (\hat{s}_i - \mathbf{z}_i^\top \beta - \gamma_i)^2 + \lambda |\gamma_i| \right]. \quad (14)$$

When all γ_i are resolved, we can directly get the closed-form estimation of β as $\hat{\beta} = (\mathbf{Z}^\top \mathbf{Z})^\dagger \mathbf{Z}^\top (\hat{\mathbf{S}} - \gamma)$. Substitute it into the objective and further define that $\tilde{\mathbf{Z}} = \mathbf{I} - \mathbf{Z}(\mathbf{Z}^\top \mathbf{Z})^\dagger \mathbf{Z}^\top$ and $\tilde{\mathbf{S}} = \tilde{\mathbf{Z}} \hat{\mathbf{S}}$, we can simplify the objective as

$$\min_{\gamma} \frac{1}{2} \|\tilde{\mathbf{S}} - \tilde{\mathbf{Z}} \gamma\|_2^2 + \lambda \|\gamma\|_1, \quad (15)$$

which is a robust linear regression problem for γ . We can then select a proper λ to solve γ and select the most reliable subset to estimate β as

$$\hat{\beta} = (\mathbf{Z}_{\text{sub}}^\top \mathbf{Z}_{\text{sub}})^\dagger \mathbf{Z}_{\text{sub}}^\top \hat{\mathbf{S}}_{\text{sub}}. \quad (16)$$

Algorithm 1: ETLT

- 1 **Input:** image $\mathbf{x}_i, 1 \leq i \leq n$, an OOD score function $S : \mathcal{X} \rightarrow \mathbb{R}$
 - 2 Calculate the features of all images $\mathbf{z}_i = g(\mathbf{x}_i)$
 - 3 Calculate the OOD score of all images $\hat{s}_i = S(\mathbf{x}_i)$
 - 4 Apply DLR to use the whole training set, or RLR to get a subset.
 - 5 $\hat{\beta} = \operatorname{argmin}_{\beta} \sum_{i \in \Gamma} (\hat{s}_i - \mathbf{z}_i^T \beta)^2$
 - 6 Compute calibrated OOD score $s_i = \mathbf{z}_i^T \hat{\beta}$
 - 7 Using s_i as the OOD score.
-

Algorithm 2: RLR

- 1 **Input:** features \mathbf{z}_i and OOD score $\hat{s}_i, 1 \leq i \leq n$,
 - 2 Normalize \mathbf{z}_i to unit Euclidean norm
 - 3 Apply dimensionality reduction on \mathbf{z}_i to $d \ll n$
 - 4 Stack \mathbf{z}_i and \hat{s}_i by rows to \mathbf{Z} and $\hat{\mathbf{S}}$
 - 5 Calculate projection $\tilde{\mathbf{Z}} = \mathbf{I} - \mathbf{Z}(\mathbf{Z}^T \mathbf{Z})^\dagger \mathbf{Z}^T$ and $\tilde{\mathbf{S}} = \tilde{\mathbf{Z}} \hat{\mathbf{S}}$
 - 6 Solving Lasso $\hat{\gamma} = \operatorname{argmin}_{\gamma} \frac{1}{2} \|\tilde{\mathbf{S}} - \tilde{\mathbf{Z}} \gamma\|_2^2 + \lambda \|\gamma\|_1$
 - 7 Select a subset $\hat{\mathbf{Z}}$ with the lowest $p\%$ of $|\hat{\gamma}_i|$.
 - 8 return $\hat{\mathbf{Z}}$
-

3.3 Online OOD detection

In the above methodology, we assume the availability of the full test set or large batch of test instances. One may judge that the test set could not be accessed fully. Therefore, we also provide an online version as per those test-time adaptation works [24, 23, 25]. The test data comes in a stream batch by batch, thus we derive a batch-wise version of our ETLT, which updates the linear model with the current and past mini-batch data iteratively. Here we illustrate the wisdom of how to estimate β online. Let us assume we have two mini-batch data pairs $(\mathbf{Z}_1, \hat{\mathbf{S}}_1), (\mathbf{Z}_2, \hat{\mathbf{S}}_2)$. Then, we can obtain two block matrices,

$$\mathbf{Z} = \begin{bmatrix} \mathbf{Z}_1 \\ \mathbf{Z}_2 \end{bmatrix}, \mathbf{S} = \begin{bmatrix} \hat{\mathbf{S}}_1 \\ \hat{\mathbf{S}}_2 \end{bmatrix}.$$

Recall that $\hat{\beta} = (\mathbf{Z}^T \mathbf{Z})^\dagger \mathbf{Z}^T \hat{\mathbf{S}}$, then we can get

$$\mathbf{Z}^T \mathbf{Z} = \begin{bmatrix} \mathbf{Z}_1^T & \mathbf{Z}_2^T \end{bmatrix} \begin{bmatrix} \mathbf{Z}_1 \\ \mathbf{Z}_2 \end{bmatrix} = \mathbf{Z}_1^T \mathbf{Z}_1 + \mathbf{Z}_2^T \mathbf{Z}_2, \quad (17)$$

$$\mathbf{Z}^T \hat{\mathbf{S}} = \begin{bmatrix} \mathbf{Z}_1^T & \mathbf{Z}_2^T \end{bmatrix} \begin{bmatrix} \hat{\mathbf{S}}_1 \\ \hat{\mathbf{S}}_2 \end{bmatrix} = \mathbf{Z}_1^T \hat{\mathbf{S}}_1 + \mathbf{Z}_2^T \hat{\mathbf{S}}_2. \quad (18)$$

When more mini-batch data pairs $(\mathbf{Z}_i, \hat{\mathbf{S}}_i)$ come, we thus can update $\mathbf{Z}^T \mathbf{Z}$ and $\mathbf{Z}^T \hat{\mathbf{S}}$ according to Algorithm. 3

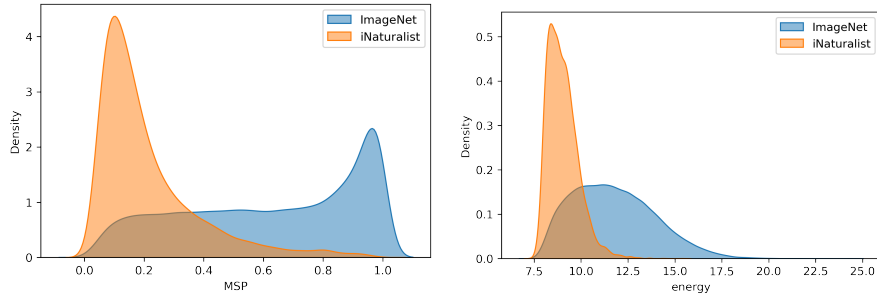


Figure 2: Kernel density estimate plot of the in- and out-of-distribution samples.

Algorithm 3: Online DLR

- 1 **Input:** an OOD score function $S : \mathcal{X} \rightarrow \mathbb{R}$, batch size b , numbers of batch m
 - 2 **Initialize:** $\mathbf{A} \leftarrow 0, \mathbf{b} \leftarrow 0$
 - 3 **for** $k = 1, \dots, m$ **do**
 - 4 Sample b images $\mathbf{x}_i, 1 \leq i \leq b$
 - 5 Calculate the features of all images $\mathbf{z}_i = g(\mathbf{x}_i)$
 - 6 Calculate the OOD score of all images $\hat{s}_i = S(\mathbf{x}_i)$
 - 7 Stack \mathbf{z}_i and \hat{s}_i by rows to \mathbf{Z} and $\hat{\mathbf{S}}$
 - 8 $\mathbf{A} \leftarrow \mathbf{A} + \mathbf{Z}^T \mathbf{Z}$
 - 9 $\mathbf{b} \leftarrow \mathbf{b} + \mathbf{Z}^T \hat{\mathbf{S}}$
 - 10 $\hat{\beta} = (\mathbf{A})^\dagger \mathbf{b}$
 - 11 Compute calibrated OOD score of the present batch $s_i = \mathbf{z}_i^T \hat{\beta}$
 - 12 **end**
 - 13 Using s_i as the OOD score.
-

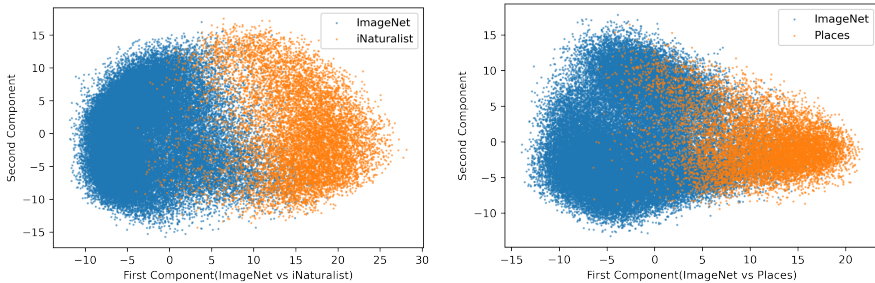


Figure 3: Visualization of features from ImageNet and two OOD datasets. The dimension of features is reduced to two by PCA.

3.4 The Linear Separability

Given an in-distribution dataset, and we sample the OOD data from a specific dataset. We empirically show that the two types of data tend to be linearly separated in Section 1. As we visualize in Fig 3, a simple unsupervised feature reduction by PCA can cluster the in-distribution and OOD data well, indicating that the feature patterns are good enough to be distinguished. Furthermore, as shown in Fig. 1, a hyper-plane can be roughly approximated to model the linear relation between the features and OOD scores. Intuitively, the linear separation comes from the definition of OOD data which has a different distribution from training dataset combined with the powerful feature extractor of neural network.

One potential issue with such linear relation modeling is that in our visualization, those feature points are not strictly on the hyper-plane. Instead, most of them are around the hyper-plane. We argue that this inconsistency is from the noisy and biased estimation given by OOD detection algorithms, otherwise no score rectification is needed. To show this, we draw OOD scores of in-distribution and out-of-distribution data using popular baseline OOD detection algorithms as in Fig. 2. This suggests that the OOD score distributions are not disjoint between in-distribution and out-of-distribution data. Hence they cannot produce a perfect OOD detection. However, we will show that these baseline OOD detector, although not powerful enough, can provide necessary information for distinguishing in- and out-of distribution data. We show that with the near linear-separable features and OOD scores, our proposed ETLT can provide a more precise OOD scoring and thus improve OOD detection, usually by a large margin.

3.5 Small Scale OOD experiments

We conduct experiments on the CIFAR-10 and CIFAR-100 datasets. Although CIFAR datasets contain easy classification images, it is hard for OOD detection due to its low resolution, especially on CIFAR-100. We use a Wide ResNet [30] of 40 layers trained on the training sets of CIFAR-10 and CIFAR-100. We use the CIFAR test set as in-distribution data and sample 2000 images from six different out-of-distribution datasets including Textures [31], SVHN [32], Places365 [33], LSUN-Crop [34], LSUN-Resize [34], and iSUN [35] following the setting in [9]. Due to randomness, we repeat 10 times trials and report the average results. We set temperature $T = 1$ for all classifiers. For ODIN, noise level is set to $\epsilon = 0.0024$. We set $p = 80$ in Algorithm 2. Besides those popular base OOD detectors, we also compare our algorithm

Table 1: Results on CIFAR datasets. The best and second best results are highlighted by the fonts of text bold and italic, respectively.

In Dataset Metric	CIFAR-10		CIFAR-100	
	FPR95↓	AUROC↑	FPR95↓	AUROC↑
Softmax	51.37	90.87	80.21	75.67
+RLR	<i>13.50</i>	<i>96.42</i>	43.73	87.06
+DLR	12.30	97.01	<i>51.63</i>	<i>84.50</i>
Energy	32.98	91.88	73.46	79.67
+RLR	16.14	95.64	58.06	82.43
+DLR	18.01	94.96	60.63	81.15
ODIN	35.77	90.96	74.55	77.23
+RLR	35.79	87.24	51.73	82.74
+DLR	37.94	86.10	51.87	81.52
KL	32.98	91.88	73.46	79.67
+RLR	16.12	95.64	58.06	82.43
+DLR	18.01	94.96	60.63	81.15
IF	79.96	62.47	80.91	66.15
LOF	95.81	56.45	98.23	43.32
GMM	87.70	58.28	94.06	69.96
GradNorm	59.84	71.65	86.55	57.56

Table 2: Results on ImageNet-1k and iNaturalist/SUN/Places/Textures datasets. The best and second best results are highlighted by the bold and italic font, respectively.

OOD Dataset Metric	iNaturalist		SUN		Places		Textures		Average	
	FPR95	AUROC	FPR95	AUROC	FPR95	AUROC	FPR95	AUROC	FPR95↓	AUROC↑
IF	88.58	61.60	90.12	57.85	93.45	50.24	54.34	87.76	81.62	64.36
LOF	95.16	51.57	94.89	52.27	93.05	56.37	82.02	65.39	91.28	56.40
GMM	87.90	68.43	89.99	63.29	96.85	52.83	95.37	35.34	92.53	54.97
GradNorm	50.03	90.33	46.48	<i>89.03</i>	60.86	84.82	61.42	<i>81.07</i>	54.70	<i>86.31</i>
MSP	63.69	87.59	79.98	78.34	81.44	76.76	82.73	74.45	76.96	79.29
+RLR	<i>21.84</i>	<i>94.87</i>	53.27	86.46	59.06	83.79	59.02	80.01	<i>48.30</i>	86.28
+DLR	21.00	94.98	<i>50.68</i>	87.13	57.16	<i>84.47</i>	<i>58.48</i>	80.24	46.83	86.71
Energy	64.91	88.48	65.33	85.32	73.02	81.37	80.87	75.79	71.03	82.74
+RLR	46.51	91.29	53.23	88.82	64.42	83.73	76.49	73.76	60.16	84.40
+DLR	45.48	91.04	52.11	88.67	62.71	84.35	69.49	75.39	57.45	84.86
KL	64.91	88.48	65.32	85.31	73.02	81.37	80.87	75.79	71.03	82.74
+RLR	46.50	91.29	53.23	88.82	64.42	83.73	76.49	73.76	60.16	84.40
+DLR	45.48	91.04	52.10	88.67	62.71	84.35	69.49	75.40	57.44	84.86
ODIN	62.69	89.36	71.67	83.92	76.27	80.67	81.31	76.30	72.99	82.56
+RLR	37.28	92.49	54.51	87.50	62.87	83.48	66.95	76.36	55.40	84.96
+DLR	34.84	92.94	51.31	92.94	<i>60.54</i>	<i>84.47</i>	66.44	76.85	53.28	85.68

with a newly proposed OOD detector GradNorm [13] and three traditional methods: Gaussian Mixture Models (GMM), Local Outlier Factor (LOF) and Isolation Forest (IF).

The results are shown in Table 1, where results show that our test time ETLT can improve the base OOD detection methods in almost all cases. Moreover, results in Table 1 show that our robust method RLR can boost the performance further. Our RLR outperforms DLR by 7.9% FPR95 and 2.56% AUROC on CIFAR-100 when using MSP as our base scoring function. Consistent improvements can be observed when using other scoring functions, such as Energy, ODIN and KL. We can also see that our DLR and RLR outperforms the other transductive methods IF, LOF and GMM and a recent state of art method GradNorm. It is worth noting that our algorithm perform even competitive with Outlier Exposure [18] and fine-tuned energy score [9], which utilize an extra outlier dataset to direct train the network to distinguish in- and out-of-distribution data.

Table 3: Results on CIFAR under different OOD detector.

In Dataset Metric Size	CIFAR-10		CIFAR-100	
	FPR95↓	AUROC↑	FPR95↓	AUROC↑
MSP	51.37	90.87	80.21	75.67
+Online DLR	15.06	96.05	55.84	83.31
Energy	32.98	91.88	73.46	79.67
+Online DLR	18.57	94.89	62.00	80.91
ODIN	35.77	90.96	74.55	77.23
+Online DLR	40.30	85.15	54.66	80.24
KL	32.98	91.88	73.46	79.67
+Online DLR	18.57	94.89	62.00	80.91

3.6 Large Scale OOD experiments

For large scale OOD detection, we use the ImageNet-1k benchmark following [13]. We use the validation set of ImageNet-1k as the in-distribution data, which consists of 50000 natural images with 1000 categories. The out-of-distribution data consist of four datasets, iNaturalist [36], SUN [37], Places [33] and Textures [31]. Google BiT-S models of ResNetV2-101 trained on ImageNet-1k is used as the feature extractor. For MSP, energy score and KL divergence, we set temperature $T = 1$. For ODIN, temperature is set to $T = 1000$, with noise level of $\varepsilon = 0$ since FGSM will not improve the results. For p in RLR, we set $p = 80$.

The results are shown in Table 2, where every OOD set are test separately and the mean results are calculated. The results show that our algorithms achieve consistent improvement over the four baseline OOD detectors. For MSP, our linear revision improve FPR95 from 76.96% to 46.83%, about the 30.13% of the improvement and outperform the state-of-the-art OOD score GradNorm by 7.87%. For AUROC, the linear calibrated MSP produce the best result, achieving equally good results as GradNorm. It seems on ImageNet-1k, the robust linear regression will not improve the results but result in slight decrease. We assume this is because the ImageNet-1k model, which was pretrained with sufficient data, owns powerful feature extraction. Thus, on ImageNet-1k OOD benchmarks the linear relation is strong enough to learn directly by DLR without the need of RLR.

3.7 Online Test-Time Training

In the previous experiments, the full test set is accessed during OOD detection, which is a special case of online test-time learning [24, 23, 25], i.e. the batch size equals the total number of test data. Here we further check how the performance varies when the batch size gets smaller, i.e. the test time data comes in stream. We compare our online DLR with those popular base OOD methods in this online setup in Table 3. From the results, we can see that our online DLR still consistently outperforms the base OOD detection methods, only except ODIN on CIFAR-10, demonstrating the efficacy of our online DLR. More importantly, the results of our online DLR are close to the results in Table 1, where the full test data set was accessed during model training. These nearly identical results clearly indicates that the effectiveness of our proposed method is not from the access of the full test set, but from the effective transductive learning regression learning as per those TTA methods [24, 23, 25].

3.8 Ablation Study

3.8.1 Effect of Subset Selection of RLR

We plot the performance improvement of our RLR as a function of the percentile of chosen subset on CIFAR-100 over two base OOD scoring metrics MSP and ODIN, as shown in Fig 4. The percentile of chosen data varies from 0.5 to 1, with step 0.05. When percentile is 1, it is equivalent to our DLR. No matter with MSP or ODIN, when we decrease the percentile, the AUROC and FPR95 improve first, which means our RLR selects proper subsets for learning the regression, eliminating the noisy samples. When we further decrease the percentile, the performances start getting worse as the training data is too limited to learn a good regressor.

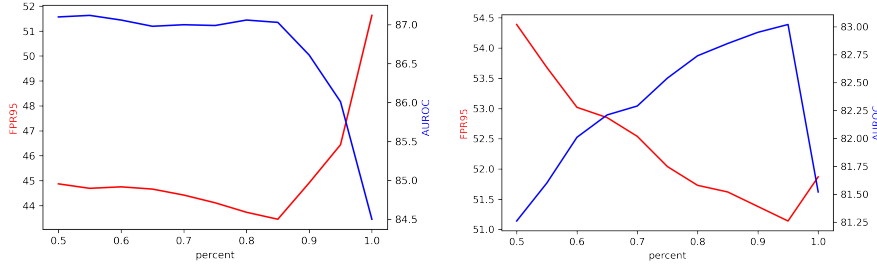


Figure 4: RLR results with different percentile of selected subset data on CIFAR-100 with MSP(left) and ODIN(right).

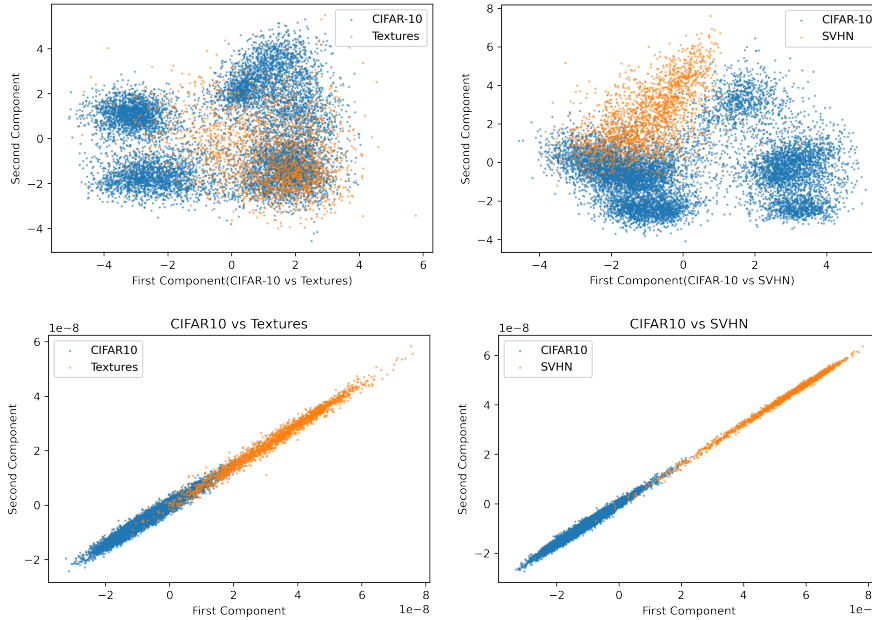


Figure 5: Visualization of feature distribution on CIFAR and OOD datasets.

3.8.2 Why RLR Failed on ImageNet-1k Benchmarks?

Similar to Section 3.4, we visualize the feature distribution on CIFAR and an OOD dataset with PCA in the first column of Fig. 5. We can see on CIFAR the separation of in- and out-of-distribution data is not as good as ImageNet-1k. This indicates that on ImageNet-1k benchmarks the feature and score linear relation is strong enough such that simple DLR can fit it well. On the contrary, filtering out subset data reduces the useful training data points, explaining why RLR failed to improve DLR in this case. However, we emphasize that the feature of CIFAR and OOD data is still roughly linearly separable, while PCA, as an unsupervised reduction method, may undermine linear separability. To better visualize the linear separability, we used LDA (with access to ground truth label) as an alternative method to reduce the dimension, and clearly display the linear separability in the second column of Fig. 5.

3.8.3 Batch Size Effect of Online DLR

We also check how the performance of our online DLR varies upon the batch size numbers. We run our online DLR with MSP in Table 4 by varying the batch size from 32 to *full* on CIFAR OOD benchmarks. From the results we can see that the performance of our online DLR is insensitive to the batch size number.

3.8.4 Combined with other methods

Recently, there are many method which can improve the OOD baseline detector. The most representative of these method is ReAct [38]. We find that our method is orthogonal to ReAct, which means they can be combined. In Table. 5 we can see our DLR outperforms ReAct with both MSP and ODIN. More interestingly, combining ReAct with DLR could get better result in some case.

Table 4: Online DLR on CIFAR with different batch size.

In Dataset Batch Size	CIFAR-10		CIFAR-100	
	FPR95↓	AUROC↑	FPR95↓	AUROC↑
Raw Softmax	51.37	90.87	80.21	75.67
32	15.06	96.05	55.84	83.31
64	15.04	96.07	55.77	83.34
128	14.99	96.10	55.64	83.38
256	14.79	96.24	55.29	83.53
512	14.53	96.38	54.79	83.69
1024	14.16	96.52	53.98	83.89
All data	12.30	97.01	51.63	84.50

Table 5: ImageNet-1k with ReAct.

Method	ReAct	DLR	FPR↓	AUROC↑
MSP	no	no	76.98	79.28
	no	yes	46.84	86.71
	yes	no	70.19	81.73
	yes	yes	67.83	81.98
ODIN	no	no	72.99	82.56
	no	yes	53.28	85.68
	yes	no	63.64	84.49
	yes	yes	48.85	87.97

3.8.5 Revision Under different in-distribution rates

From this section on, we only utilize DLR and focus on how linear calibration can improve the baseline OOD detector. On CIFAR-10 and CIFAR-100, we tried to change the rate of in-distribution data for OOD detection. The rate of in-distribution data vary from 5% to 95% in Fig. 6, with spacing 5%. We fix the total number of data at 5000 because some out of distribution have less than 10000 images. Every experiment is repeated 10 times and the average is used as the final results. We find that using MSP or energy as base OOD detector, our linear revision succeed in making correct classification with some improvements even with only 20% to 40% of in-distribution data. When the rate of

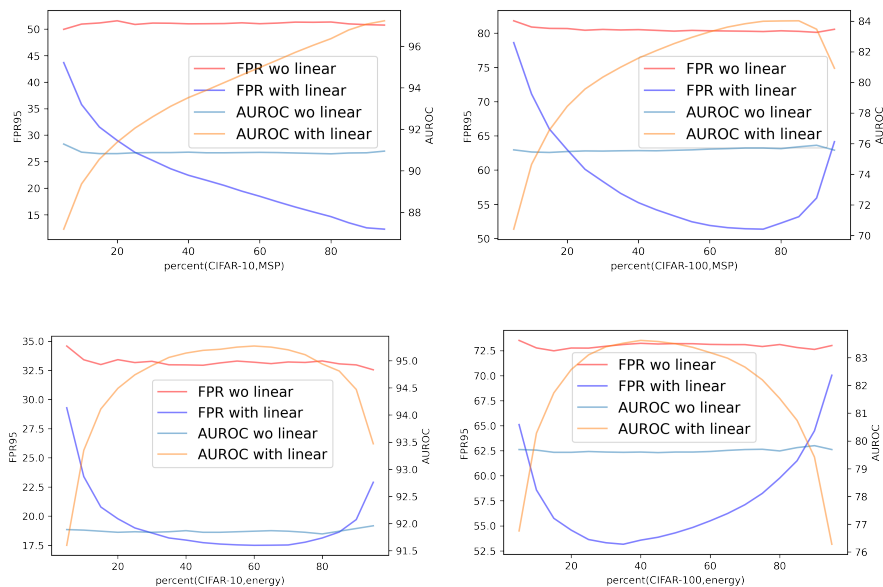


Figure 6: Results under different in-distribution rate

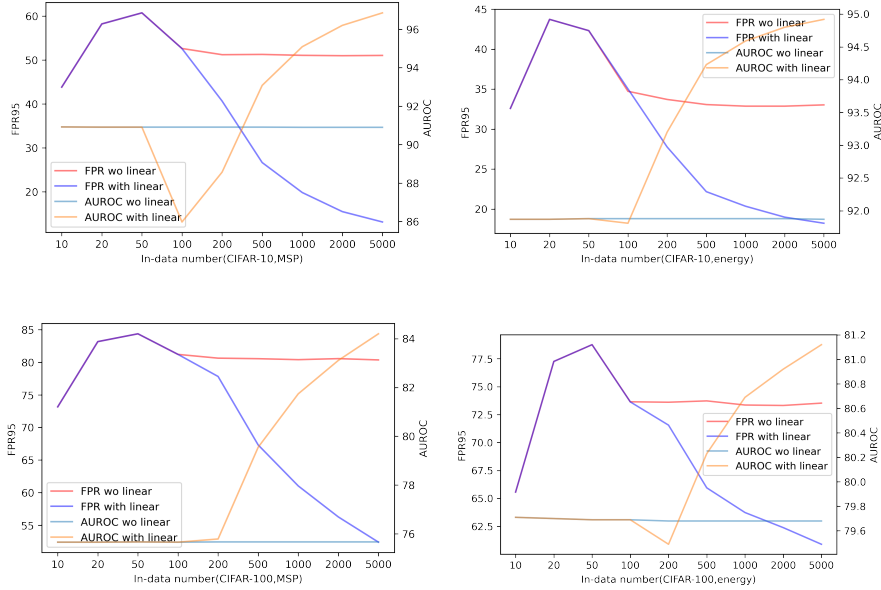


Figure 7: Results under different total sample number

in-distribution get smaller, our proposed linear revision will instead worsen the results. This is because when there is too small number of in-distribution, it is hard to capture the rich information of in-distribution. However, this is still astonishing because our methods still work when in-distribution only account for a small part of the all observation, where the classical outlier detection methos. We argue that this is because we utilized the information of pre-trained classifiers. Even if in-distribution data compose of the smaller part of dataset during OOD testing, OOD scores tend to produce larger scores for inliers and lower score for outliers, and linear regression will keep this tendency.

3.8.6 Revision Under different sample number

Still on CIFAR, we keep the rate of in-distribution data and out-of-distribution data at 5:1, then change the total number of in-distribution from 10000 to 10 in Fig. 7. It is worth noting that we repeat more rounds when the total sample number is smaller to get more accurate estimation. Let’s denote m as the number of in-distribution data fed in the test time. We correspondingly repeat $\frac{10^5}{m}$ rounds. We find that when number of test data is too small (around the dimension of feature, note that the penultimate layer of Wide ResNet-40 of CIFAR use 128-dimensional), our algorithms will produce no revision because it fit the OOD score perfectly. When the number of data grow, our linear revision may first decease AUROC. However, our algorithm consistently improve the results when there are more than 500 in-distribution samples.

3.8.7 Extend the results with multiple OOD data sets

Because all the above experiments carried out on single datasets then take average over all datasets, we wonder if our methods work when multi out-of-distribution domains is simultaneously given during. We carry out experiments on large scale OOD detection, fix the ImageNet-1k validation set as in-distribution. The out-of-distribution data are all the combination of iNaturalist, Places, SUN and Texturs datasets (shorted as NPST). The results are visualized in Fig. 8 We find that our DLR can improve on all the combination of the given four datasets.

3.8.8 Results on Noise

Sometimes, noises are more challenging than disjointed datasets as OOD data. We also test how our DLR can help in these cases. We test two kind of noise, Gaussian noise with $\mu = 0.5$ clipped to $[0, 1]$ and Uniform noise between $[0, 1]$. The results are shown in Tab. 6. Without DLR, both MSP and ODIN can not distinguish in- and out-of-distribution data easily. After applying DLR, the results greatly improve.

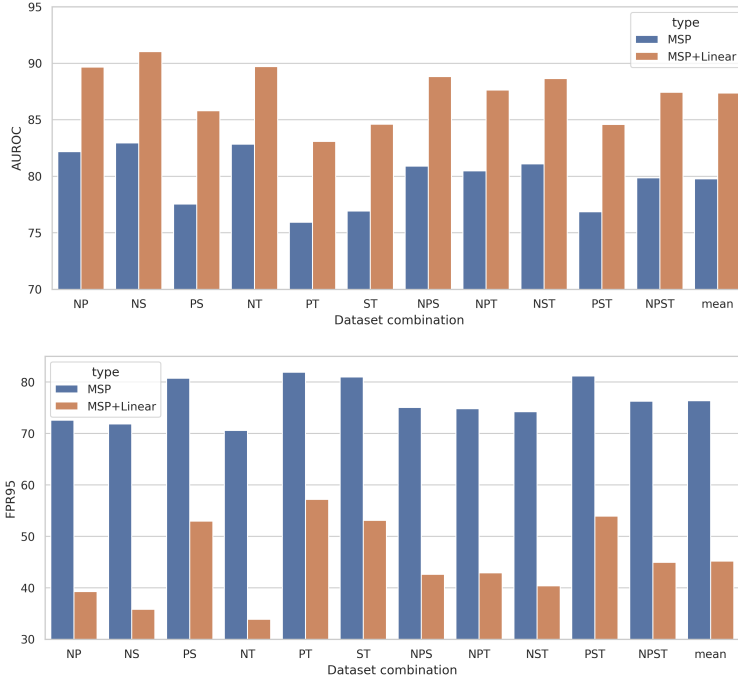


Figure 8: Results of Combination of Datasets

Table 6: Results on Noise.

Method	Noise	FPR↓	AUROC↑
MSP	Uniform	99.60	89.13
	Gaussian	99.77	88.08
MSP+DLR	Uniform	0.01	99.50
	Gaussian	0.01	99.34
ODIN	Uniform	99.14	90.12
	Gaussian	99.56	89.15
ODIN+DLR	Uniform	7.05	97.29
	Gaussian	15.38	96.73

4 Conclusion

In this paper, we find that a roughly linear relation between features extracted by deep neural networks and their OOD scores produced by those popular OOD detection algorithms on various standard OOD datasets. Thus an embarrassingly simple test-time linear training model (ETLT) is proposed to discover and exploit this linear relation for OOD scores prediction directly based on the input feature, including DLR and a robust variant RLR. Though simple, our ETLT methods outperform those popular OOD detection methods and achieve new the state-of-the-art performance on many benchmarks.

References

- [1] Karen Simonyan and Andrew Zisserman. Very deep convolutional networks for large-scale image recognition. *arXiv preprint arXiv:1409.1556*, 2014.
- [2] Kaiming He, Xiangyu Zhang, Shaoqing Ren, and Jian Sun. Deep residual learning for image recognition. *CoRR*, 2015.
- [3] Gao Huang, Zhuang Liu, Laurens Van Der Maaten, and Kilian Q Weinberger. Densely connected convolutional networks. In *Proceedings of the IEEE conference on computer vision and pattern recognition*, pages 4700–4708, 2017.
- [4] Alexey Dosovitskiy, Lucas Beyer, Alexander Kolesnikov, Dirk Weissenborn, Xiaohua Zhai, Thomas Unterthiner, Mostafa Dehghani, Matthias Minderer, Georg Heigold, Sylvain Gelly, et al. An image is worth 16x16 words: Transformers for image recognition at scale. *arXiv preprint arXiv:2010.11929*, 2020.
- [5] Anh Nguyen, Jason Yosinski, and Jeff Clune. Deep neural networks are easily fooled: High confidence predictions for unrecognizable images. In *Proceedings of the IEEE conference on computer vision and pattern recognition*, pages 427–436, 2015.
- [6] Sunil Thulasidasan, Gopinath Chennupati, Jeff A Bilmes, Tanmoy Bhattacharya, and Sarah Michalak. On mixup training: Improved calibration and predictive uncertainty for deep neural networks. *Advances in Neural Information Processing Systems*, 32, 2019.
- [7] Dan Hendrycks and Kevin Gimpel. A baseline for detecting misclassified and out-of-distribution examples in neural networks. *arXiv preprint arXiv:1610.02136*, 2016.
- [8] Yen-Chang Hsu, Yilin Shen, Hongxia Jin, and Zsolt Kira. Generalized odin: Detecting out-of-distribution image without learning from out-of-distribution data. In *Proceedings of the IEEE/CVF Conference on Computer Vision and Pattern Recognition*, pages 10951–10960, 2020.
- [9] Weitang Liu, Xiaoyun Wang, John D Owens, and Yixuan Li. Energy-based out-of-distribution detection. *arXiv preprint arXiv:2010.03759*, 2020.
- [10] Kimin Lee, Kibok Lee, Honglak Lee, and Jinwoo Shin. A simple unified framework for detecting out-of-distribution samples and adversarial attacks. *Advances in neural information processing systems*, 31, 2018.
- [11] Engkarat Techapanurak, Masanori Suganuma, and Takayuki Okatani. Hyperparameter-free out-of-distribution detection using cosine similarity. In *Proceedings of the Asian Conference on Computer Vision*, 2020.
- [12] Jie Ren, Stanislav Fort, Jeremiah Liu, Abhijit Guha Roy, Shreyas Padhy, and Balaji Lakshminarayanan. A simple fix to mahalanobis distance for improving near-ood detection. *arXiv preprint arXiv:2106.09022*, 2021.
- [13] Rui Huang, Andrew Geng, and Yixuan Li. On the importance of gradients for detecting distributional shifts in the wild. *arXiv preprint arXiv:2110.00218*, 2021.
- [14] Shiyu Liang, Yixuan Li, and Rayadurgam Srikant. Enhancing the reliability of out-of-distribution image detection in neural networks. *arXiv preprint arXiv:1706.02690*, 2017.
- [15] Kimin Lee, Honglak Lee, Kibok Lee, and Jinwoo Shin. Training confidence-calibrated classifiers for detecting out-of-distribution samples. *arXiv preprint arXiv:1711.09325*, 2017.
- [16] Ian J Goodfellow, Jonathon Shlens, and Christian Szegedy. Explaining and harnessing adversarial examples. *arXiv preprint arXiv:1412.6572*, 2014.
- [17] Terrance DeVries and Graham W Taylor. Learning confidence for out-of-distribution detection in neural networks. *arXiv preprint arXiv:1802.04865*, 2018.
- [18] Dan Hendrycks, Mantas Mazeika, and Thomas Dietterich. Deep anomaly detection with outlier exposure. *arXiv preprint arXiv:1812.04606*, 2018.
- [19] Marc Masana, Idoia Ruiz, Joan Serrat, Joost van de Weijer, and Antonio M Lopez. Metric learning for novelty and anomaly detection. *arXiv preprint arXiv:1808.05492*, 2018.
- [20] Jiefeng Chen, Yixuan Li, Xi Wu, Yingyu Liang, and Somesh Jha. Atom: Robustifying out-of-distribution detection using outlier mining. In *Joint European Conference on Machine Learning and Knowledge Discovery in Databases*, pages 430–445. Springer, 2021.
- [21] Sina Mohseni, Mandar Pitale, JBS Yadawa, and Zhangyang Wang. Self-supervised learning for generalizable out-of-distribution detection. In *Proceedings of the AAAI Conference on Artificial Intelligence*, volume 34, pages 5216–5223, 2020.

- [22] Aristotelis-Angelos Papadopoulos, Mohammad Reza Rajati, Nazim Shaikh, and Jiamian Wang. Outlier exposure with confidence control for out-of-distribution detection. *Neurocomputing*, 441:138–150, 2021.
- [23] Yu Sun, Xiaolong Wang, Zhuang Liu, John Miller, Alexei Efros, and Moritz Hardt. Test-time training with self-supervision for generalization under distribution shifts. In *International Conference on Machine Learning*, pages 9229–9248. PMLR, 2020.
- [24] Dequan Wang, Evan Shelhamer, Shaoteng Liu, Bruno Olshausen, and Trevor Darrell. Tent: Fully test-time adaptation by entropy minimization. *arXiv preprint arXiv:2006.10726*, 2020.
- [25] Yusuke Iwasawa and Yutaka Matsuo. Test-time classifier adjustment module for model-agnostic domain generalization. *Advances in Neural Information Processing Systems*, 34, 2021.
- [26] Xuefeng Hu, Gokhan Uzunbas, Sirius Chen, Rui Wang, Ashish Shah, Ram Nevatia, and Ser-Nam Lim. Mixnorm: Test-time adaptation through online normalization estimation. *arXiv preprint arXiv:2110.11478*, 2021.
- [27] Marvin Zhang, Sergey Levine, and Chelsea Finn. Memo: Test time robustness via adaptation and augmentation. *arXiv preprint arXiv:2110.09506*, 2021.
- [28] Guansong Pang, Chunhua Shen, Longbing Cao, and Anton Van Den Hengel. Deep learning for anomaly detection: A review. *ACM Computing Surveys (CSUR)*, 54(2):1–38, 2021.
- [29] Yann LeCun, Sumit Chopra, Raia Hadsell, M Ranzato, and F Huang. A tutorial on energy-based learning. *Predicting structured data*, 1(0), 2006.
- [30] Sergey Zagoruyko and Nikos Komodakis. Wide residual networks. *arXiv preprint arXiv:1605.07146*, 2016.
- [31] Mircea Cimpoi, Subhansu Maji, Iasonas Kokkinos, Sammy Mohamed, and Andrea Vedaldi. Describing textures in the wild. In *Proceedings of the IEEE Conference on Computer Vision and Pattern Recognition*, pages 3606–3613, 2014.
- [32] Yuval Netzer, Tao Wang, Adam Coates, Alessandro Bissacco, Bo Wu, and Andrew Y Ng. Reading digits in natural images with unsupervised feature learning. 2011.
- [33] Bolei Zhou, Agata Lapedriza, Aditya Khosla, Aude Oliva, and Antonio Torralba. Places: A 10 million image database for scene recognition. *IEEE transactions on pattern analysis and machine intelligence*, 40(6):1452–1464, 2017.
- [34] Fisher Yu, Ari Seff, Yinda Zhang, Shuran Song, Thomas Funkhouser, and Jianxiong Xiao. Lsun: Construction of a large-scale image dataset using deep learning with humans in the loop. *arXiv preprint arXiv:1506.03365*, 2015.
- [35] Pingmei Xu, Krista A Ehinger, Yinda Zhang, Adam Finkelstein, Sanjeev R Kulkarni, and Jianxiong Xiao. Turkergaze: Crowdsourcing saliency with webcam based eye tracking. *arXiv preprint arXiv:1504.06755*, 2015.
- [36] Grant Van Horn, Oisin Mac Aodha, Yang Song, Yin Cui, Chen Sun, Alex Shepard, Hartwig Adam, Pietro Perona, and Serge Belongie. The inaturalist species classification and detection dataset. In *Proceedings of the IEEE conference on computer vision and pattern recognition*, pages 8769–8778, 2018.
- [37] Jianxiong Xiao, James Hays, Krista A Ehinger, Aude Oliva, and Antonio Torralba. Sun database: Large-scale scene recognition from abbey to zoo. In *2010 IEEE computer society conference on computer vision and pattern recognition*, pages 3485–3492. IEEE, 2010.
- [38] Yiyu Sun, Chuan Guo, and Yixuan Li. React: Out-of-distribution detection with rectified activations. *Advances in Neural Information Processing Systems*, 34:144–157, 2021.

Appendix A Experiments Setting

For all results except for changing the percentile of chosen data in RLR, we set the regularization $\lambda = 1e - 5$ and chosen percentile $p = 80\%$. For experiments on CIFAR-10 and CIFAR-100, we directly use the feature of the penultimate layer of Wide ResNet-40. On ImageNet-1k, we further apply principal component analysis to the output of penultimate layer of ResNetv2-101, to reduce the dimension of feature to 64. For GMM model on CIFAR-10 and CIFAR-100, we use Gaussian mixtures of 10 and 100 components respectively, and each component has its own general covariance matrix. For GMM model on ImageNet-1k, a Gaussian Mixture of 1000 components with diagonal covariance matrix is used. The log-likelihood of each sample is used as an OOD score. For local outlier factor model, we set number of neighbors to 20. For Isolation Forest, the number of base estimators is set to 100.

Appendix B Detailed results on ImageNet-1k and CIFAR

Here we list the detailed results of experiments on every single OOD datasets, which is omitted in the paper due to page limitation. The results of ImageNet-1k, CIFAR-10 and CIFAR-100 are displayed respectively in Tab. 7, Tab. 8, Tab. 9.

Table 7: Detailed Experiments on ImageNet-1k with AUPR

Dataset metrics	iNaturalist			SUN		
	FPR95	AUROC	AUPR	FPR95	AUROC	AUPR
MSP	63.69	87.59	97.23	79.98	78.34	94.45
+RLR	21.84	94.87	98.69	53.27	86.46	96.44
+DLR	21.00	94.98	98.71	50.68	87.13	96.61
Energy	64.91	88.48	97.58	65.33	85.32	96.57
+RLR	46.51	91.29	98.07	53.23	88.82	97.50
+DLR	45.48	91.04	97.96	52.11	88.67	97.38
KL	64.91	88.48	97.58	65.32	85.31	96.57
+RLR	46.50	91.29	98.07	53.23	88.82	97.50
+DLR	45.48	91.04	97.96	52.10	88.67	97.38
ODIN	62.69	89.36	97.76	71.67	83.92	96.26
+RLR	37.28	92.49	98.27	54.51	87.50	97.01
+DLR	34.84	92.94	98.37	51.31	92.94	97.26
GradNorm	50.03	90.33	97.83	46.48	89.03	97.29
GMM	87.90	68.43	90.26	89.99	63.29	88.72
LOF	95.16	51.57	83.87	94.89	52.27	84.04
IF	88.58	61.60	87.92	90.12	57.85	86.09

Dataset metrics	Places			Textures		
	FPR95	AUROC	AUPR	FPR95	AUROC	AUPR
MSP	81.44	76.76	94.15	82.73	74.45	95.65
+RLR	59.06	83.79	95.75	59.02	80.01	96.22
+DLR	57.16	84.47	95.94	58.48	80.24	96.30
Energy	73.02	81.37	95.49	80.87	75.79	96.05
+RLR	64.42	83.73	96.01	76.49	73.76	95.57
+DLR	62.71	84.35	96.14	69.49	75.39	95.47
KL	73.02	81.37	95.49	80.87	75.79	96.05
+RLR	64.42	83.73	96.01	76.49	73.76	95.57
+DLR	62.71	84.35	96.14	69.49	75.40	95.47
ODIN	76.27	80.67	95.35	81.31	76.30	96.12
+RLR	62.87	83.48	95.84	66.95	76.36	95.58
+DLR	60.54	84.47	96.11	66.44	76.85	95.71
GradNorm	60.86	84.82	96.26	61.42	81.07	96.96
GMM	96.85	52.83	84.54	95.37	35.34	83.83
LOF	93.05	56.37	85.64	82.02	65.39	92.77
IF	93.45	50.24	83.02	54.34	87.76	98.27

Table 8: Details of Experiments On CIFAR-10

Dataset Method	Textures			SVHN			Places365		
	FPR	AUROC	AUPR	FPR	AUROC	AUPR	FPR	AUROC	AUPR
MSP	59.50	88.37	97.16	48.98	91.86	98.26	60.32	88.08	97.08
+RLR	27.35	91.89	97.33	11.24	95.91	98.46	31.49	93.22	98.32
+DLR	20.83	94.56	98.43	10.47	96.71	98.96	29.86	93.46	98.40
Energy	52.33	85.36	95.48	35.49	91.15	97.72	40.16	89.75	97.25
+RLR	34.74	88.52	95.97	10.28	97.38	99.32	35.82	91.33	97.76
+DLR	36.75	87.23	95.44	14.64	95.73	98.80	37.55	90.76	97.64
Odin	49.62	84.57	95.14	32.88	92.11	98.03	57.14	84.23	95.73
+RLR	53.33	77.01	91.57	27.00	88.96	95.87	55.31	84.24	95.71
+DLR	60.74	72.08	89.53	27.18	89.31	96.10	63.96	80.08	94.40
KL	52.34	85.36	95.48	35.49	91.15	97.72	40.17	89.75	97.25
+RLR	34.69	88.53	95.98	10.29	97.39	99.32	35.74	91.33	97.76
+DLR	36.74	87.23	95.44	14.67	95.74	98.80	37.55	90.75	97.63
GradNorm	73.59	57.90	83.12	59.49	70.21	89.45	78.38	60.51	86.99
GMM	60.24	83.07	95.80	98.01	23.62	70.12	80.85	79.14	94.97
IF	99.35	21.64	70.19	78.71	67.98	89.67	91.94	55.09	85.27
LOF	96.90	45.94	80.20	92.86	57.39	86.12	98.62	52.92	84.58
Dataset Method	LSUN-C			LSUN-R			iSUN		
	FPR	AUROC	AUPR	FPR	AUROC	AUPR	FPR	AUROC	AUPR
MSP	30.95	95.63	99.13	52.23	91.49	98.17	56.24	89.80	97.73
+RLR	0.50	99.83	99.96	2.08	99.51	99.89	8.33	98.17	99.57
+DLR	0.18	99.92	99.98	3.73	99.19	99.82	8.75	98.19	99.59
Energy	8.31	98.34	99.65	27.75	94.15	98.65	33.84	92.51	98.23
+RLR	0.56	99.81	99.94	5.79	98.81	99.74	9.69	97.98	99.55
+DLR	1.44	99.61	99.89	7.05	98.58	99.69	10.62	97.87	99.54
Odin	15.90	96.98	99.33	26.63	94.58	98.77	32.45	93.29	98.48
+RLR	39.79	84.25	94.56	17.82	94.81	98.53	21.46	94.14	98.40
+DLR	37.13	85.77	95.23	19.65	94.32	98.41	18.96	95.08	98.69
KL	8.31	98.34	99.65	27.75	94.15	98.65	33.84	92.51	98.23
+RLR	0.56	99.81	99.94	5.81	98.81	99.74	9.67	97.98	99.55
+DLR	1.42	99.61	99.89	7.02	98.58	99.69	10.62	97.87	99.54
GradNorm	12.07	96.85	99.18	65.27	73.38	92.06	70.27	71.07	91.41
GMM	96.12	46.31	80.17	95.84	58.68	89.29	95.10	58.88	89.14
IF	59.47	82.96	95.11	71.85	76.06	93.43	78.44	71.09	91.75
LOF	97.62	51.69	83.89	94.21	65.72	90.49	94.64	65.04	90.08

Table 9: Details of Experiments On CIFAR-100

Dataset Method	Textures			SVHN			Places365		
	FPR	AUROC	AUPR	FPR	AUROC	AUPR	FPR	AUROC	AUPR
MSP	83.55	73.67	93.07	84.00	71.44	92.89	82.30	74.03	93.30
+RLR	57.25	80.62	93.02	44.29	84.18	94.93	76.63	76.16	93.53
+DLR	64.26	78.55	92.87	56.75	78.72	93.42	75.19	76.47	93.59
Energy	79.32	76.40	93.70	85.43	73.96	93.62	80.11	75.80	93.59
+RLR	69.14	74.68	91.39	63.51	77.91	93.67	77.56	75.87	93.51
+DLR	70.08	73.51	91.29	64.85	78.73	94.23	80.46	73.55	92.84
Odin	79.57	73.43	92.81	87.73	65.43	90.95	87.14	72.00	92.67
+RLR	69.01	76.09	92.60	77.75	68.83	90.10	86.30	70.30	91.79
+DLR	65.44	74.61	92.13	67.50	69.81	89.50	88.29	68.33	91.21
KL	79.32	76.40	93.70	85.43	73.96	93.62	80.11	75.80	93.59
+RLR	69.14	74.68	91.39	63.51	77.91	93.67	77.56	75.87	93.51
+DLR	70.08	73.51	91.29	64.85	78.73	94.23	80.46	73.55	92.84
GradNorm	87.48	60.41	87.46	97.30	55.00	86.83	96.95	53.65	85.83
GMM	92.18	63.26	89.34	99.09	62.07	91.35	86.33	73.32	92.46
IF	95.44	49.11	82.42	79.60	72.67	92.35	87.76	62.94	88.68
LOF	98.47	42.35	80.32	98.08	44.98	83.38	99.26	38.93	80.28
Dataset Method	LSUN-C			LSUN-R			iSUN		
	FPR	AUROC	AUPR	FPR	AUROC	AUPR	FPR	AUROC	AUPR
MSP	66.00	83.85	96.35	82.48	75.39	94.08	82.93	75.62	94.10
+RLR	20.12	96.09	99.14	33.99	92.43	98.21	30.10	92.88	98.22
+DLR	19.68	96.18	99.15	48.24	88.13	97.11	45.66	88.94	97.28
Energy	35.78	93.46	98.60	79.14	79.42	95.04	81.00	78.99	94.92
+RLR	25.53	94.94	98.86	56.23	85.66	96.46	56.42	85.53	96.40
+DLR	27.81	93.83	98.51	59.68	83.83	95.98	60.90	83.43	95.85
Odin	57.38	87.05	97.07	69.27	82.48	95.81	66.22	83.01	95.85
+RLR	29.64	94.12	98.67	23.89	93.72	98.32	23.78	93.36	98.10
+DLR	34.32	92.95	98.37	28.50	91.66	97.67	27.18	91.79	97.57
KL	35.78	93.46	98.60	79.14	79.42	95.04	81.00	78.99	94.92
+RLR	25.53	94.94	98.86	56.23	85.66	96.46	56.42	85.53	96.40
+DLR	27.80	93.83	98.51	59.68	83.83	95.98	60.90	83.43	95.85
GradNorm	39.47	92.12	98.22	99.06	40.06	80.11	99.06	44.09	82.10
GMM	92.69	68.75	91.34	96.17	78.01	95.34	97.93	74.34	94.19
IF	40.69	90.68	97.72	90.66	60.69	88.15	91.32	60.79	88.44
LOF	97.37	36.64	77.84	98.02	49.36	85.27	98.16	47.67	84.65